Optical tomography system based on second-differential spectroscopy for small animal brain study

Heng Xu, Hamid Dehghani, Brian W. Pogue, Keith D. Paulsen
[1]*Thayer School of Engineering, Dartmouth College, Hanover NH 03755*
(Email: heng.xu@dartmouth.edu, Tel:(603) 646-2859, Fax:(603) 646-3856)

Roger Springett, Jeff F. Dunn
Dartmouth Medical School,, Hanover, NH 03755

Abstract: An 8-Channel broadband spectroscopy and tomography CCD system was designed and frequency domain reconstruction was applied to get both absorption and scattering images at two wavelengths based on the second-differential spectroscopy analysis of CW data.

OCIS codes: (170.6960) Tomography (170.6510) Spectroscopy (170.3880) Medical and biological imaging

1. Introduction

Near infrared spectroscopy have been widely accepted as a successful tool to quantify and monitor tissue hemodynamics and oxygenation in a noninvasive fashion. In order to better understand the pathology and function of the brain, we developed a multi-channel broadband spectroscopy system to study the temporal response of rat brain and also employed multi-source-detector configuration to realize tomography imaging. Although our system only measures DC spectra, the differential pathlengths at 740nm and 840nm can be calculated using second-differential spectroscopy analysis. With both intensity and pathlength information, scattering and absorption images can be simultaneously reconstructed at these wavelengths and to allow hemoglobin and oxygen saturation distribution estimation.

2. Method

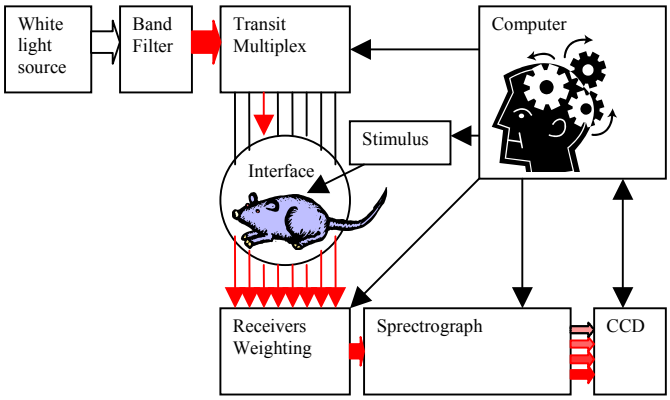

Figure 1: Diagram of the system

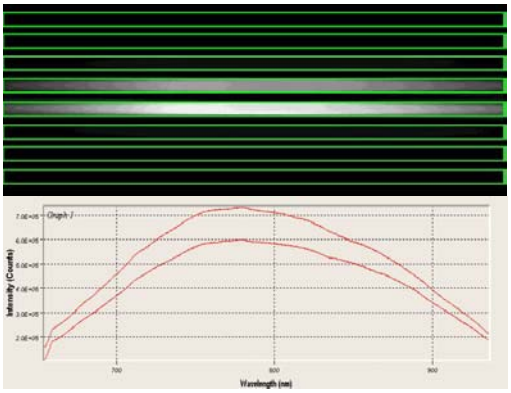

Figure 2: (a) Image on the CCD (b) corresponding intensity spectrum

2.1 Instrumentation

A 100W DC-regulated broadband quartz halogen lump is used as a light source. The beam is first filtered by a set of glass filters and narrowed to the interested waveband. This unit endows the system the ability to do either NIRS or visible spectroscopy. Then the beam is passed through 8 transmit fibers simultaneously and multiplexed by a rotating shutter. The source is turned on sequentially and attenuated through the object and collected simultaneously by 8 receive fibers. The receive fibers are passed through another rotating stage on which a neutral density wheel is installed to balance the light intensity in each fiber. Then the 8 fibers are sorted in a line vertically and focused on the spectrograph. In the spectrograph, the light is horizontally separated by wavelength through a grating. Finally the dispersed beams form an eight-strip pattern and fall onto the CCD chip. The CCD converts the photons to electrons

and sends the maps to computer. Typical images from CCD camera are shown in Figure 2(a). The rectangles define the areas to sample the 8 received beams. By summing the column pixel together, we can get the spectrum of the corresponding receiver, shown in Figure 2(b), x-axis is wavelength and y-axis is intensity (unit: counts of electrons).

2.2 Second-differential Spectroscopy

Matcher et al described a method to measure differential pathlength (DP) by a similar system using second-differential spectroscopy fitting[1]. Our method is based on this, but instead of starting from modified Beer-Lambert law, we used a mathematically more rigorous derivation where the assumptions are more transparent and easier to examine. Because the attenuation A is determined by the optical properties $\mu_a(\lambda), \mu_s(\lambda)$ and both the absorption and scattering coefficients are wavelength dependent, so the attenuation also is wavelength dependent. For the second differential analysis, we can expand $A(\mu_a(\lambda), \mu_s(\lambda))$ with respect to λ as:

$$\frac{\partial^2 A}{\partial \lambda^2} = \frac{\partial A}{\partial \mu_a}\frac{\partial^2 \mu_a}{\partial \lambda^2} + \frac{\partial^2 A}{\partial {\mu_a}^2}\left(\frac{\partial \mu_a}{\partial \lambda}\right)^2 + \frac{\partial A}{\partial \mu_s}\frac{\partial^2 \mu_s}{\partial \lambda^2} + \frac{\partial^2 A}{\partial {\mu_s}^2}\left(\frac{\partial \mu_s}{\partial \lambda}\right)^2 \quad (1)$$

It has been found that, with the chromophores present in tissue and with the weak wavelength dependence of scattering coefficient of tissue, the last three terms are small compared to the first term. Given that the absorption coefficient is determined by the makeup of the chromophores and their extinction coefficients and replace $\partial A / \partial \mu_a$ with the term DP, we get $\frac{\partial^2 A}{\partial \lambda^2} = \sum_{i=1}^{Nc}\left(DP \cdot C_i \frac{\partial^2 \varepsilon_i}{\partial \lambda^2}\right)$. If we discretize it into a certain wavelength range λ_i ($i = 1, \cdots, n$), we could get a matrix form Eq. (2):

$$\begin{bmatrix} \frac{\partial^2 A}{\partial \lambda^2}(\lambda_1) \\ \vdots \\ \frac{\partial^2 A}{\partial \lambda^2}(\lambda_n) \end{bmatrix} = \begin{bmatrix} DP(\lambda_1)\cdot\frac{\partial^2 \varepsilon_1}{\partial \lambda^2}(\lambda_1) & \cdots & DP(\lambda_1)\cdot\frac{\partial^2 \varepsilon_{Nc}}{\partial \lambda^2}(\lambda_1) \\ \vdots & \ddots & \vdots \\ DP(\lambda_n)\cdot\frac{\partial^2 \varepsilon_1}{\partial \lambda^2}(\lambda_n) & \cdots & DP(\lambda_n)\cdot\frac{\partial^2 \varepsilon_{Nc}}{\partial \lambda^2}(\lambda_n) \end{bmatrix} \cdot \begin{bmatrix} C_1 \\ \vdots \\ C_{Nc} \end{bmatrix} \quad (2)$$

$$\begin{bmatrix} \frac{\partial^2 A}{\partial \lambda^2}(\lambda_1) \\ \vdots \\ \frac{\partial^2 A}{\partial \lambda^2}(\lambda_n) \end{bmatrix} = \begin{bmatrix} \frac{\partial^2 \varepsilon_1}{\partial \lambda^2}(\lambda_1) & \cdots & \frac{\partial^2 \varepsilon_{Nc}}{\partial \lambda^2}(\lambda_1) \\ \vdots & \ddots & \vdots \\ \frac{\partial^2 \varepsilon_1}{\partial \lambda^2}(\lambda_n) & \cdots & \frac{\partial^2 \varepsilon_{Nc}}{\partial \lambda^2}(\lambda_n) \end{bmatrix} \cdot \overline{DP} \cdot \begin{bmatrix} C_1 \\ \vdots \\ C_{Nc} \end{bmatrix} \quad (3)$$

The DP is wavelength-dependent. Assuming its variation is insignificant in a small wavelength range and can be approximated to a single value $\overline{DP}$, one obtains Eq. (3). Now, the right side matrix can be reduced to the second differential extinction coefficient spectra which are well known. Applying multilinear regression method, we can obtain $\overline{DP}$ scaled concentrations, $\overline{DP} \cdot C_i$ ($i = 1, \cdots, N_c$). Since one of the important chromophores, water, can be measured by other technologies accurately (i.e., the water concentration C_w is well known). $\overline{DP}$ can be extracted out from $\overline{DP} \cdot C_w$. Consequently other chromophore concentrations could also be derived. We define this estimate of $\overline{DP}$ as DPW, which is the differential pathlength near the wavelength of a water peak. Here, a very important assumption is that the water is distributed homogeneously in the medium that seems reasonable in the rat head case where the major tissues brain and muscles have very similar water content [2]. A detailed discussion about the water heterogeneity can be found in else where [3]. Examining the second differential spectrum of the water extinction coefficient, three significant features exist in the near infrared range, respectively near 740nm, 840nm and 950nm. In our broadband system, we choose ranges 700-800nm and 800-880nm to fit. Therefore, DPW around 740nm and 840nm can be estimated and further we can estimate the absolute concentration of other chromospheres or monitor the dynamics from baseline by converting the measured attenuation into changes of concentration in the spectroscopy study.

2.3 Frequency domain Image Reconstruction

It has been shown that when the modulation frequency was under 200MHz, the attenuation measured at several centimeters varied very little and the phase shift was almost equivalent to the differential pathlength[4]. Therefore, it is possible to map the CW measurements into frequency domain at least at these two wavelengths, 740nm and 840nm [3]. Then we can take the advantage of frequency domain reconstruction to get both absorption and scattering tomographic images at two wavelengths and monitor the hemodynamics spatially. We use a finite element model for the approximation of light propagation in tissue and for image reconstruction using measured boundary data [5].

3. Results

Phantom studies were performed to validate the models and to test the system. We started with phantoms of fresh rat blood and intralipid saline solution. The hemoglobin concentration was quantified using a co-oximeter.. The scattering of Intralipid can be calculated using the formula from van Staveren el al. [6] The oxygenation also can be

controlled by either yeast or pumped oxygen. Therefore the optical property spectra of the mixture can be predicted. The reconstructed absorption coefficient linearly correlated to the change of blood concentration when the background scattering was unchanged. The reconstructed scattering coefficient also linearly correlated to the changes of intralipid concentration when the absorption was unchanged. We also found that there was a small offset between the reconstructed and predicted absorptions and there were both offset and scaling shifts in the scattering coefficient. These offsets and scaling factors were probably introduced by the model misfit error. These factors could be reduced using calibrations. When this was done, it is possible to obtain an accurate measurement of the hemoglobin concentration from the absorption measured at 740nm and 840nm. Figure 3 shows the comparison of estimated versus predicted concentration in either full-oxygenated or full-deoxygenated situations. Next, we also imaged some liquid phantoms embedded with strong absorbing heterogeneity. As we show in Figure 4, the object could be reconstructed at the true position while the value seemed to be underestimated if the object was in the center.

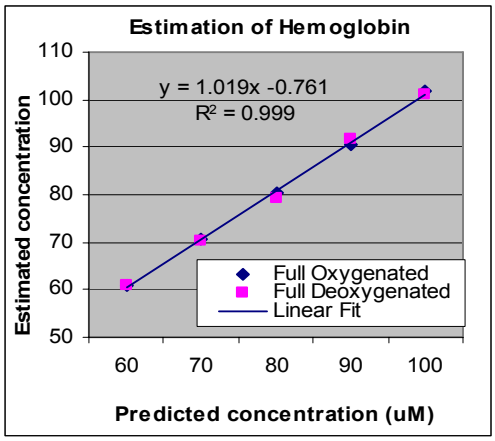

Figure 3, Hemoglobin concentration estimation

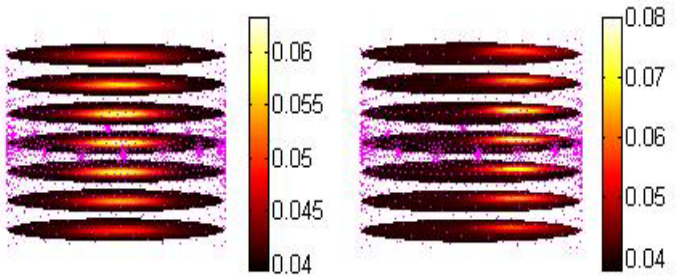

Figure 4, Examples of heterogeneous phantom reconstruction.

4. Discussion

In this report, we have described a multi-channel broadband both spectroscopy and tomography system. Based on second-differential spectroscopy, both absorption and scattering images can be reconstructed using frequency domain method. In the future, more experiments need to be done to evaluate the system and improve the reconstruction algorithm.

5. Acknowledgements

This work has been sponsored by the National Institute of Health through grants NIH RO1 NS38471 and RO1 CA69544.

6. References

1. Matcher, S.J., M. Cope, and D.T. Delpy, *Use of the water absorption spectrum to quantify tissue chromophore concentration changes in near-infrared spectroscopy.* Phys Med Biol, 1994. **39**(1): p. 177-96.
2. Reinoso, R.F., B.A. Telfer, and M. Rowland, *Tissue water content in rats measured by desiccation.* J Pharmacol Toxicol Methods, 1997. **38**(2): p. 87-92.
3. Xu, H., Pogue, B.W., Dehghani, H., Springett, R., Paulsen, K.D., Dunn, J.F., *Feasibility of NIR tomographic reconstruction with multispectral continuous wave data by mapping into frequency domain data.* Proc. SPIE, 2003. **4955-16**.
4. Arridge, S.R., Cope, M., Delpy, D. T., *The theoretical basis for the determination of optical pathlengths in tissue: temporal and frequency analysis.* Phys. Med. Biol., 1992. **37**(7): p. 1531-1560.
5. Xu, H., et al., *Near-infrared imaging in the small animal brain: optimization of fiber positions.* J Biomed Opt, 2003. **8**(1): p. 102-10.
6. van Staveren, H.J., et al., *Light Scattering in Intralipil-10% in the wavelength range of 400-1100nm.* Applied Optics, 1991. **30**(31): p. 4507-4514.